JOURNAL OF MATERIALS SCIENCE 14 (1979) 1447–1456

Flux growth of crystals of some transition metal fluorides

Part 2

B. M. WANKLYN, F. R. WONDRE, A. MAQSOOD*, K. YANAGISAWA†
Clarendon Laboratory, Oxford, UK
W. DAVISON
School of Physics, University of Newcastle upon Tyne, UK

The flux growth of crystals of the following complex fluorides is reported: $KAlF_4$, $KMnF_3$, $RbFeF_4$, Rb_2FeF_5, Rb_3FeF_6, Rb_xFeF_3 ($0.18 < x < 0.29$), $CsFeF_4$, $CsFe_2F_7$, $Cs_3Fe_2F_9$, Cs_xFeF_3 ($0.18 < x < 0.29$), Na_2CoFeF_7, Na_2NiFeF_7, Na_2NiAlF_7, Na_2ZnCrF_7, $NaCrF_4$ and $Rb_2Cr_5F_{17}$. Flux impurity levels, determined by electron probe microanalysis (EPMA), were low. However, attempts to produce $BaNiF_4$, $BaCoF_4$, $CsCrF_4$ and $Cs_2Cr_5F_{17}$ resulted in crystals with higher levels of substitutional impurities. X-ray powder patterns and EPMA were used to characterize the crystals.

1. Introduction

Many complex fluorides of the transition metals have been prepared as powder specimens because of interest in their magnetic properties. The flux growth method has previously been successfully used to prepare crystals of some of these materials [1–4] and its further application is reported in this paper. In Table I, the reported magnetic transition temperatures of some of the materials described here are listed [5–16]. The compounds containing Fe^{2+} or Fe^{3+} are especially useful for investigation by the Mössbauer method.

Of the compounds reported in this paper, $KMnF_3$ [17] is known to melt congruently and thus can be grown as crystals from the pure melt. This method produces large crystals relatively rapidly, but has two disadvantages: firstly, considerable amounts of pure, oxide-free starting materials are essential, and secondly, the dislocation density is usually of the order of 10^3 to 10^4 cm^{-2} [18], as compared with 10^2 cm^{-2} for flux-grown complex fluorides [19, 20]. Zone-refined MnF_2 and CoF_2 can be obtained, but commercially available FeF_2, FeF_3, CrF_3 and NiF_2 contain oxides as well as adsorbed water.

TABLE I Magnetic transition temperatures of some complex fluorides

Formula	T_N (K)	Reference
$KMnF_3$	275, 280, 253	[5–7]
$RbFeF_4$	134	[8]
Rb_2FeF_5	14.2	[9]
$CsFeF_4$	159	[10]
Rb_xFeF_3 ($0.18 < x < 0.29$)	80, 116	[11, 12]
Cs_xFeF_3 ($0.18 < x < 0.29$)	116	[12]
Na_2NiFeF_7	90 (T_c)	[13]
Na_2NiAlF_7	90	[14]
$BaNiF_4$	150	[15]
$BaCoF_4$	69.6	[16]

The flux growth of Na_2CoFeF_7 and Na_2NiFeF_7 from $NaCl–MCl_2$ has been reported [21]. However, the crystals were small, and in the present work alternative flux systems have been investigated. The other complex fluorides reported here containing FeF_2, FeF_3 and CrF_3 have not previously been prepared as single crystals, with the exception of $RbFeF_4$ [4], for which a new starting composition is given. Many of these compounds cannot be grown from a pure melt because they melt incongruently. The flux method has, however, been shown to be suitable for such compounds since hydrofluorination of oxide impurities in the starting materials is readily accomplished by the addition of NH_4HF_2 [1–4, 22].

*Present address: Physics Department, Quaid-i-Azam University, Islamabad, Pakistan.
†Present address: Industrial Materials Research Laboratory, Tokyo Institute of Technology, Tokyo, Japan.

TABLE II Starting compositions, cooling programmes and crystal products
(a)

Batch no.	Compounds obtained	Starting composition (g)	Crucible volume (cm^3)	Initial temperature (° C)	Rate of cooling ($K\,h^{-1}$)	Final temperature (° C)	Crystal products
1	$KAlF_4$	3.6 AlF_3, 6.1 KHF_2, 10.7 $PbCl_2$, 4 NH_4HF_2	20	750	5	350	Transparent colourless platelets up to 4 mm × 4 mm × 2 mm (Fig. 1)
2	$KMnF_3$	9.7 MnF_2, 11.6 KF, 38.5 $PbCl_2$, 3.5 NH_4HF_2	50	950	3	415 ("hot drained")	Transparent, rectangular, pale pink, up to 8 mm × 5 mm × 5 mm (with inclusions)
3	$RbFeF_4$	12.8 FeF_3, 20.3 RbF, 26.8 $PbCl_2$, 10.7 NH_4HF_2	50	740	5	300	Colourless to orange translucent plates up to 15 mm × 15 mm × 0.3mm
4	Rb_2FeF_5 and Rb_3FeF_6	9.4 FeF_3, 20.9 RbF 20 $PbCl_2$, 7 NH_4HF_2	50	680	1.8	340 ("hot drained" at 540)	Faceted colourless rods of Rb_2FeF_5, transparent, up to 3.5 mm × 2 mm × 1 mm
5	$CsFeF_4$	13.5 FeF_3, 20.2 CsCl, 14.7 PbF_2, 9.3 $PbCl_2$ 7 NH_4HF_2	50	630	4	300	Milky crystals, 1.5 mm on edge, at crucible walls Purplish or brownish plates, up to 7 mm × 7 mm × 0.2 mm (Fig. 4)
6	$CsFeF_4$ and $Cs_3Fe_2F_9$	9 FeF_3, 25 Cl, 16.5 PbF_2, 7 NH_4HF_2	50	640	2.6	300	Orange-brown $CsFeF_4$, transparent, 1.5 mm × 2mm × 3 mm, near base. Colourless, hexagonal, fragile platelets of $Cs_3Fe_2F_9$ at surface and throughout melt, up to 4 mm × 4 mm × 0.5 mm
7	$CsFe_2F_7$	6 FeF_2, 4.8 CsCl, 18 PbF_2, 5.3 NH_4HF_2	20	950	7	350	Large black plates, up to 8 mm × 6 mm × 0.5 mm, at melt surface, and 2 mm octahedra on wall and base of crucible
8	Rb_xFeF_3 $(0.18 < x < 0.29)$	5.7 FeF_3, 2.1 RbF, 21.8 $PbCl_2$, 3.0 NH_4HF_2	20	870	5	520 ("hot drained")	Black, shiny, brittle hexagonal rods, up to 2 mm × 2 mm × 8 mm (Fig. 3)
9	Cs_xFeF_3 $(0.18 < x < 0.29)$	5.9 FeF_3, 3.2 CsF, 21.8 $PbCl_2$, 2.0 NH_4HF_2	20	840	10	450 ("hot drained)	Black, shiny, brittle hexagonal rods, up to 1 mm × 1 mm × 5 mm

(b)

Compounds obtained	Starting composition (g)	Crucible volume (cm^3)	Initial temperature (° C)	Rate of cooling ($K\,h^{-1}$)	Final temperature (° C)	Crystal products
Na_2CoFeF_7	1.3 CoF_2, 1.5 FeF_3, 1.7 $NaHF_2$, 3.5 $PbCl_2$, 2.0 NH_4HF_2	20	870	10	300	Large, pinkish-brown crystals, intergrown
Na_2NiFeF_7	6.5 NiF_2, 7.8 FeF_3, 8.5 $NaHF_2$ 17.5 $PbCl_2$, 8 NH_4HF_2	50	957	4	300	Large, shiny, dark-brown, intergrown crystals, up to 10 mm × 10 mm × 6 mm
Na_2NiAlF_7	6.5 NiF_2, 5.5 AlF_3, 8.5 $NaHF_2$, 17.5 $PbCl_2$, 8 NH_4HF_2	50	957	4	300	Pale green intergrown crystals (Fig. 5)
Na_2ZnCrF_7	6.7 ZnF_2, 7.5 CrF_3, 8.5 $NaHF_2$, 17.5 $PbCl_2$, 8 NH_4HF_2	40	957	4	300	Dark green pseudocubes at surface of melt
$NaCrF_4$	6.6 CrF_3, 3.7 $NaHF_2$, 20.0 $PbCl_2$, 3.2 NH_4HF_2	20	957	4	300	Faceted transparent rods, up to 3.5 mm × 1.0 mm × 0.5 mm, and platelets
β $RbCrF_4$	6.8 CrF_3, 5.1 RbCl, 4.2 RbF, 3.0 NH_4HF_2	20	870	10	300	Green, fibrous β $RbCrF_4$ covering the surface of the melt
$Rb_2Cr_5F_{17}$	6.6 CrF_3, 6.3 RbF, 20.0 $PbCl_2$, 3.1 NH_4HF_2	20	957	4	300	Clumps of brownish green fibres at the melt surface. At the crucible walls, dark green crystals which cleaved easily, up to 2.0 mm × 2.0 mm × 8 mm (Fig. 6)
(Ba, Pb) $Ni(F, Cl)_4$	5.0 NiF_2, 10.0 BaF_2, 8.6 PbF_2, 42.5 $PbCl_2$, 3.5 NH_4HF_2	50	1000	4	600	A layer of light green rods at the melt surface, up to 6 mm × 2 mm × 0.5 mm
(Ba, Pb) $Co(F, Cl)_4$	6.0 CoF_2, 14.0 BaF_2, 8.6 PbF_2, 38.5 $PbCl_2$, 3.5 NH_4HF_2	50	860	4	300	Small purple rods, up to 3 mm × 0.5 mm × 0.2 mm
(Cs, Pb) CrF_4 and $(Cs, Pb)_2Cr_{4.6}F_{17}$	7.9 CrF_3, 12.08 CsCl, 8.8 $PbCl_2$, 8.8 PbF_2, 4.0 NH_4HF_2	20	954	7	350	Long, brownish-green needles Irregular, dark, brownish-green platelets

For identification purposes, a thesis by Tressaud [23] has been particularly helpful. He prepared powder specimens by reacting the purified components in sealed tubes of platinum or gold, and characterized the compounds by X-ray powder patterns. He also determined melting points and, in some cases, magnetic transition temperatures.

2. Chemicals and equipment

The chemicals used were: Koch Light FeF_3 and MnF_2; BDH Laboratory Reagent grade $NaHF_2$, BaF_2, KHF_2, CsF, CsCl, RbF, NH_4HF_2 and $PbCl_2$; BDH "Optran" AlF_3, CoF_2, NiF_2 and ZnF_2; BDH "Analar" CsCl; BDH "Extra Pure" PbF_2; and Cambrian Chemicals CrF_3. Platinum crucibles of 0.5 mm wall thickness with close-fitting lids were used. The crucibles were heated in D-shaped sillimanite muffles to protect the crusilite elements from attack by flux vapours [24].

3. Experimental details

The materials were weighed, mixed, placed in crucibles and the lids fitted as closely as possible. The crucibles were placed on a layer of alumina powder in the sillimanite muffle and the entrance was blocked with refractory brick. The furnace was heated to the desired initial temperature and slow cooling was commenced at once.

The starting compositions and furnace programmes which produced the best crystals are given in Tables IIa and b.

4. Results

X-ray powder patterns of the crystals were compared with published data. When crystals could not be identified in this way, an empirical formula was derived from EPMA. The more reactive fluorides of the transition metals proved to be difficult subjects for EPMA since they did not polish well, had poor conductivity, and hydrolysed readily on exposure to air.

All the compounds contained iron hydrolysed in water, and mechanical methods of separation from the flux were thus necessary; accordingly, the crystals were broken out of the solid flux and scraped clean with a razor-blade, or the flux was "hot-drained" from the crucible while molten, by inverting the crucible and heating to a temperature above the eutectic.

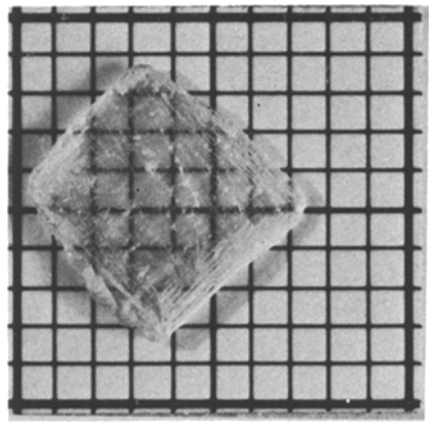

Figure 1 Platelet of $KAlF_4$ (mm grid).

5. Notes on the crystals

5.1. $KAlF_4$

The crystals were colourless, transparent plates up to 4 mm x 4 mm x 2 mm, and were soft and easy to bend, like $KFeF_4$ [4]. Viewed perpendicularly to the surfaces, they were optically isotropic. They reacted with water, forming $Al(OH)_3$. One is shown in Fig. 1.

5.2. $KMnF_3$

The crystals were transparent, pale pink, with rectangular facets. The larger crystals contained flux inclusions, but some smaller ones (e.g. 2 mm x 2 mm x 3 mm) showed no strain and were free from visible inclusions.

5.3. Compounds in the system FeF_3–RbF–$PbCl_2$

The starting compositions that produced the crystals indicated are shown in the triangular composition diagram (Fig. 2a). The crystals are described below.

5.3.1. $RbFeF_4$

The previously reported composition for flux growth of $RbFeF_4$ contained FeF_3, RbCl and RbF [4]. The composition reported here contains FeF_3, RbF and $PbCl_2$, and yielded thin plates up to 15 mm x 15 mm, which were larger in area than those obtained earlier. They appeared twinned under the polarizing microscope, and this was

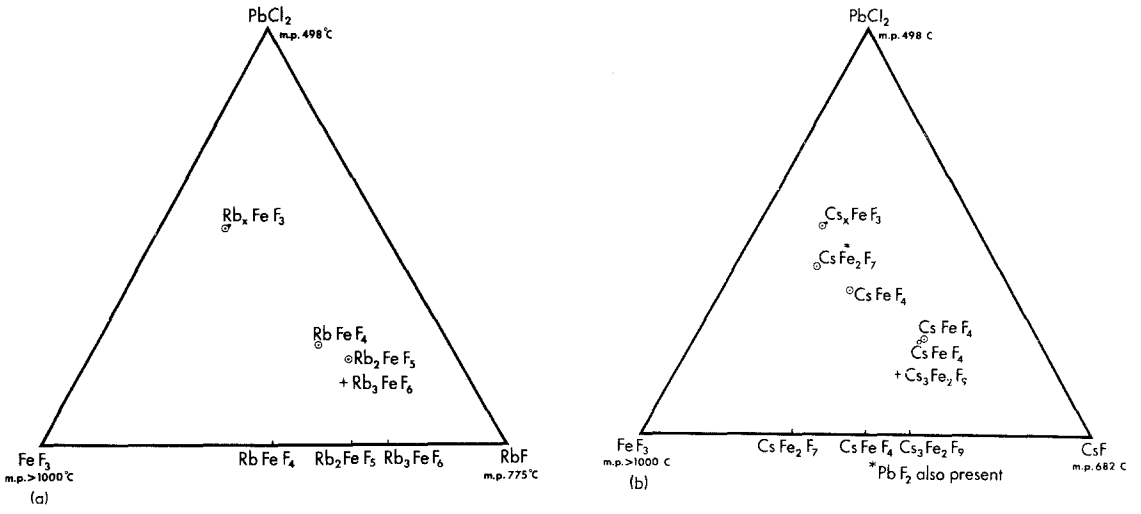

Figure 2 (a) Triangular composition diagram for the system FeF_3–RbF–$PbCl_2$, showing starting compositions that produced the compounds indicated. (b) Triangular composition diagram for the system FeF_3–CsF–$PbCl_2$, showing starting compositions that produced the compounds indicated.

confirmed by Lâue back-reflection photographs. The twinning results from crystallographic transitions below the growth temperature [25].

5.3.2. Rb_2FeF_5

Rb_2FeF_5 was obtained from composition 5, Table IIa, which produced also Rb_3FeF_6. The crucible was "hot-drained" at 520° C. The crystals of Rb_2FeF_5 were faceted rods with rough surfaces, up to 3.5 mm x 2 mm x 1 mm. The rods were colourless and transparent; carefully selected crystals showed simultaneous extinction. The Mössbauer spectrum showed no sign of Fe^{2+}.

5.3.3. Rb_3FeF_6

This material could easily be distinguished from the transparent rods of Rb_2FeF_5, which were also present, since it formed a layer of closely packed, milky crystals, each about 1.5 mm in all dimensions, at the crucible wall. Apparently, Rb_3FeF_6 crystallized first, followed at a later stage by Rb_2FeF_5. Under the polarizing microscope, it could be seen that extinction occurred. No crystallographic facets were evident.

EPMA indicated that the Rb:Fe molar ratio was 2.99:1, in good agreement with the formula Rb_3FeF_6. X-ray powder pattern data are given in Table III.

TABLE III X-ray powder pattern data for Rb_3FeF_6

Intensity, estimated	d_{obs} (Å)
VW	5.9
W	3.59
VW	3.49
VW	3.27
VS	3.15
VW	2.896
VW	2.700
W	2.571
VW	2.337
S	2.227
S	1.823
VW	1.776

5.3.4 $\alpha Rb_x FeF_3$ $(0.18 < x < 0.29)$

The structure of this material is very similar to that of $Rb_2Fe_5F_{17}$ [26], and both closely resemble that of the tungsten bronze αM_xWO_3. Thus it is very difficult to distinguish between αRb_xFeF_3 and $Rb_2Fe_5F_{17}$ by X-ray methods. The powder patterns have identical d-values and similar intensities except for a few of the weaker lines [26, 27].

The Rb_xFeF_3 crystals were obtained as black, shiny, brittle hexagonal rods (Fig. 3) when the starting temperature was 870° C, while lower starting temperatures (near 650° C) gave a platy habit. Mössbauer experiments showed that crystals of both habits contained Fe^{2+} and Fe^{3+} in a ratio corresponding to the formula Rb_xFeF_3 $(0.18 < x < 0.29)$, or approximately $RbF \cdot FeF_2 \cdot 3FeF_3$. The X-ray powder pattern was in close agreement with that of $Rb_{0.28}FeF_3$ [27].

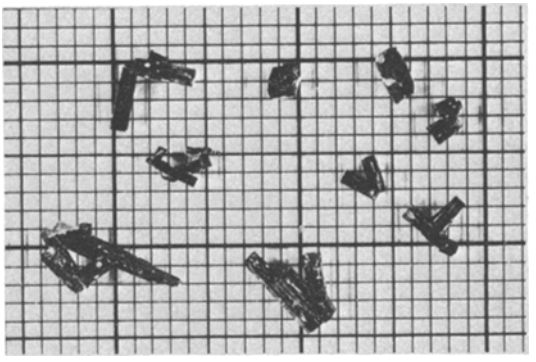

Figure 3 Rods of Rb_xFeF_3 (mm grid).

5.4. Compounds in the system FeF_3–CsF–$PbCl_2$

The starting compositions that produced the crystals indicated are shown in the triangular composition diagram (Fig. 2b). Notes on the crystals follow.

5.4.1. $CsFeF_4$

Large, thin plates resulted from starting composition 5. They were transparent, purplish or brownish, and cleaved less readily than $KFeF_4$ and $RbFeF_4$. Thicker crystals of $CsFeF_4$, transparent and up to 1.5 mm thick, resulted from composition 6. Some are shown in Fig. 4. The X-ray powder pattern data are given in Table IV. Mössbauer experiments showed that no Fe^{2+} was present in the crystals.

5.4.2. $Cs_3Fe_2F_9$

Composition 7 produced a second phase in the form of colourless, triangular or hexagonal platelets up to 4 mm x 4 mm x 0.5 mm at the melt surface, and also large thin sheets throughout the melt.

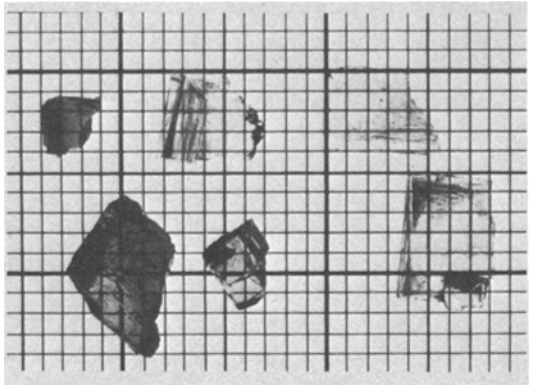

Figure 4 Platelets of $CsFeF_4$ (mm grid).

TABLE IV X-ray powder patter data for $CsFeF_4$

Intensity, estimated	hkl	d_{obs} (Å)	$d_{calc.}$ (Å)
VW	0 1 0	6.580	6.56
VS	0 1 2	3.345	3.345
M	0 2 0	3.275	3.278
M	2 0 2	2.748	2.740
MW	2 1 2	2.539	2.533
MW	2 2 0	2.503	2.498
W	2 2 2	2.099	2.102
MW	0 0 4	1.944	1.944
MW	2 3 0	1.903	1.902
MW	2 1 4	1.682	1.680
VW	0 4 0	1.645	1.640
VW	2 3 4	1.360	1.360

$a_0 = 7.73$ Å, $b_0 = 6.56$ Å, $c_0 = 7.78$ Å

Since they reacted with water and were fragile, it was not possible to recover the sheets intact. EPMA (Table V) was in good agreement with the formula $Cs_3Fe_2F_9$ and showed very low impurity levels. This material had previously been prepared only as a powder, and the published unit cell dimensions and space group [28] were used to index the X-ray powder pattern obtained from single crystal material, which is given in Table VI. Mössbauer experiments showed that Fe^{2+} was almost certainly absent.

TABLE V Composition of $Cs_3Fe_2F_9$ confirmed by EPMA

	Formula requires (%)	EPMA indicates (%)
Cs	58.5	57.2
Fe	16.4	16.4
F	25.1	24.2
Pb		0.03
Cl		0.01

TABLE VI X-ray powder pattern data for $Cs_3Fe_2F_9$

Intensity, estimated	$hkil$	d_{obs} (Å)	d_{calc} (Å)
S	$10\bar{1}3$	3.66	3.66
S	$11\bar{2}0$	3.16	3.17
VW	$10\bar{1}4$	3.06	3.06
W	0 0 0 6	2.462	2.462
VS	$20\bar{2}3$	2.395	2.397
VW	$10\bar{1}6$	2.249	2.246
VW	$10\bar{1}7$	1.974	1.970
VW	$11\bar{2}6$	1.941	1.944
W	$21\bar{3}3$	1.910	1.911
M	$30\bar{3}0$	1.828	1.829
MS	$22\bar{4}0$	1.585	1.584
W	$31\bar{4}3$	1.455	1.454

$a_0 = 6.335$ (2) Å $c_0 = 14.77$ (2) Å ($P\bar{6}2c$ [28])

5.4.3. $CsFe_2F_7$

Large black plates grew at the melt surface and smaller black octahedra, 2 mm on edge, were found on the wall and base of the crucible.

The ratio Cs:Fe, determined by EPMA, was 1:1.9. The Mössbauer spectrum indicated that iron was present almost entirely as Fe^{3+}, and that two sites are present in the unit cell. The EPMA and Mössbauer spectrum are thus both in agreement with the formula $CsFe_2F_7$, with two sites for Fe^{3+}. A structure analysis has been undertaken [29]. Laue photographs showed that the octahedra examined were single crystals. X-ray powder pattern data have been indexed similarly to pyrochlore [30] and are given in Table VII.

TABLE VII X-ray powder pattern data for $CsFe_2F_7$

Intensity, estimated	hkl	d_{obs} (Å)	d_{calc} (Å)
M	2 2 0	3.66	3.66
VS	3 1 1	3.13	3.13
W	2 2 2	2.993	2.992
VW	4 0 0	2.591	2.591
W	3 3 1	2.377	2.378
VW	4 2 2	2.115	2.116
S	3 3 3	1.996	1.995
S	4 4 0	1.833	1.833
W	6 2 0	1.640	1.639
W	5 3 3	1.581	1.581
VW	6 2 2	1.562	1.563

a_0 = 10.37 Å

5.4.4. Cs_xFeF_3 $(0.18 < x < 0.29)$

Cs_xFeF_3 has a structure very similar to $Cs_2Fe_5F_{17}$ [14]; thus, like the Rb analogue, it closely resembles the tungsten bronze structure. It is similarly difficult to distinguish between these two forms on the basis of X-ray methods. The crystals gave an X-ray powder pattern which agreed closely with data obtained from a sintered sample [23]. The indexed powder pattern, obtained from single crystal material, is given in Table VIII.

TABLE VIII X-ray powder pattern data for Cs_xFeF_3 $(0.18 < x < 0.29)$

Intensity, estimated	$hkil$	d_{obs} (Å)	d_{calc} (Å)
MW	0 0 0 2	3.813	3.815
S	$1\,0\,\bar{1}\,2$	3.286	3.286
VS	$2\,0\,\bar{2}\,0$	3.246	3.235
M	$1\,1\,\bar{2}\,2$	2.678	2.669
W	$2\,1\,\bar{3}\,0$	2.445	2.445
W	$2\,1\,\bar{3}\,2$	2.060	2.059
M	$3\,0\,\bar{3}\,2$	1.872	1.867
MW	$3\,0\,\bar{3}\,3$	1.654	1.654
VW	$4\,0\,\bar{4}\,2$	1.486	1.489
VW	$2\,2\,\bar{4}\,4$	1.338	1.334
VW	$4\,1\,\bar{5}\,3, 4\,0\,\bar{4}\,4$	1.239	1.234

a_0 = 7.47 Å, c_0 = 7.63 Å.

5.5. Na_2ABF_7

Crystals with A = Mn, Ni and Co, B = Fe, Al, have previously been prepared from NaCl + MCl_2 as flux, in sealed platinum crucibles [21]. In the present experiments, $PbCl_2$ was used as flux in crucibles with well-fitting lids. The yields were large and, because the crystals were intergrown, only a few were faceted. They were soft and rather fragile. Some of these compounds are described below.

5.5.1. Na_2CoFeF_7

The crystals were brownish pink, translucent, and up to 5 mm x 4 mm x 3 mm in size. Extinction was not simultaneous. The X-ray powder pattern agreed with published data [31] and EPMA was in good agreement with the formula, indicating only 0.1% Cl and 0.3% Pb in the crystal (Table IX). However, EPMA showed, in addition, many small precipitates of $PbCl_2$ throughout the crystal. Mössbauer experiments indicated the absence of Fe^{2+}.

5.5.2. Na_2NiFeF_7

The shiny dark-brown crystals, up to 10 mm x 10 mm x 6 mm, cleaved easily. Under the polarizing microscope, smaller platelets appeared yellow and showed simultaneous extinction. Some small octahedra were also present. The X-ray powder pattern agreed with ASTM data [32]. Mössbauer experiments again indicated the absence of Fe^{2+}.

5.5.3. Na_2NiAlF_7

The crystals were soft, brittle and pale green. Some were rod-shaped, while others were pseudocubic, and the smaller crystals showed simultaneous extinction. Some NiF_2 crystals grew at the crucible base; these were a brighter, yellowish green. X-ray powder pattern data for crystals of Na_2NiAlF_7 are given in Table X, and some are shown in Fig. 5.

5.5.4 Na_2ZnCrF_7

A layer of dark green crystals grew at the surface of the melt and separate pseudocubic crystals up to 2 mm x 2 mm x 2 mm were attached to the crucible walls. Under the polarizing microscope,

TABLE IX EPMA data for crystals of Na_2CoFeF_7

Na_2CoFeF_7	requires (%)	EPMA indicates (%)
Na	15.7	15.9
Co	19.0	19.4
Fe	20.1	20.9
F	45.3	43.9
Cl		0.1
Pb		0.3

the crystals were seen to be intimately twinned. X-ray powder pattern data are given in Table X.

5.6. $NaCrF_4$

The crystals grew as dark green, faceted, platy rods up to 3.5 mm x 1.0 mm x 0.5 mm. Under the polarizing microscope, most showed simultaneous extinction but twinned regions were visible in some. The X-ray powder pattern was in good agreement with ASTM data [33].

5.7. $\beta RbCrF_4$

The surface of the solidified melt was covered with microscopic needles. The X-ray powder pattern of these needles agreed with ASTM data [34].

5.8. $Rb_2Cr_5F_{17}$

These crystals grew as brownish-green fibrous aggregates, up to 8 mm x 2 mm x 2 mm. Extinction was not uniform. Some are shown in Fig. 6.

TABLE X X-ray powder pattern data for Na_2NiAlF_7 and Na_2ZnCrF_7

Intensity, estimated	*hkl*	Na_2NiAlF_7		Na_2ZnCrF_7	
		d_{obs} (Å)	d_{calc} (Å)	d_{obs} (Å)	d_{calc} (Å)
VS	011	5.95	5.92	6.02	6.09
MS	101	5.10	5.09	5.20	5.20
MS	121	3.58	3.58	3.66	3.67
S	031, 211	3.04	3.05	3.11	3.12
VS	022	2.962	2.962	3.00	3.04
VS	220	2.892	2.894	2.966	2.956
W	202	2.548	2.546	2.591	2.601
VW	040	2.515	2.515		
W	013	2.375	2.374		
VW	132	2.335	2.335		
W	103	2.311	2.309	2.374	2.369
W	222	2.273	2.271	2.322	2.325
M	113	2.249	2.251	2.305	2.309
VW	123	2.100	2.099		
W	042	2.075	2.074		
VW	321	2.050	2.050	2.096	2.092
MS	033	2.173	2.174	2.041	2.031

a_0 = 7.077 Å a_0 = 7.198 Å
b_0 = 10.06 Å b_0 = 10.37 Å
c_0 = 7.329 Å c_0 = 7.526 Å

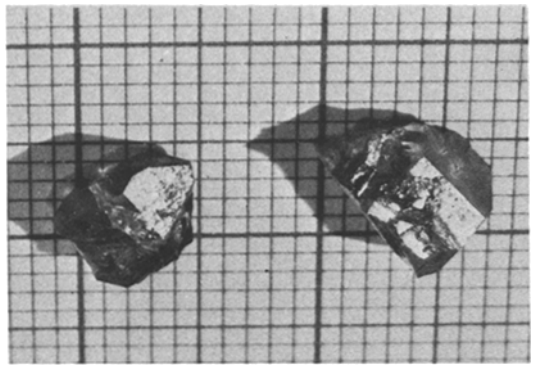

Figure 5 Crystals of Na_2NiAlF_7 (mm grid).

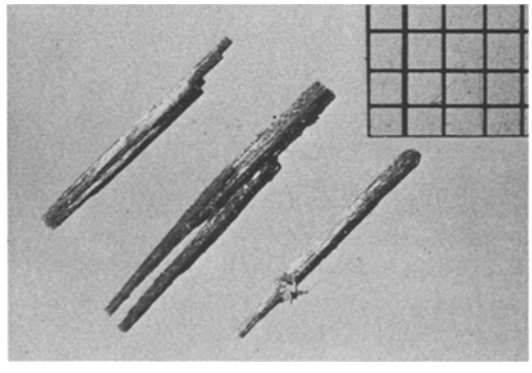

Figure 6 Needles of $Rb_2Cr_5F_{17}$ (mm grid).

The X-ray powder pattern resembled that of $K_2V_5F_{17}$ [35]. EPMA was in good agreement with the formula $Rb_2Cr_5F_{17}$, with only 0.9% Pb and 0.3% C in the crystal (Table XI).

5.9. (Cs, Pb) CrF_4

The crystals grew as dark green rods up to 6 mm x 0.5 mm x 0.5 mm, with hexagonal facets.

The X-ray powder pattern differed from that published for $CsCrF_4$ [36]. EPMA showed a considerable amount of Pb in the lattice, and was in good agreeement with the empirical formula $(Cs_{0.6}Pb_{0.2})\ CrF_4$ (Table XII).

5.10. $(Cs, Pb)_2Cr_{4.6}F_{17}$

The batch which produced (Cs, Pb) CrF_4 also yielded irregularly shaped, brownish-green platelets, typically 2 mm x 3 mm x 0.5 mm. They were transparent and highly twinned. The X-ray powder pattern data differed from that published for $Cs_2Cr_5F_{17}$ [37], and EPMA showed the presence of a large amount of Pb in the lattice (Table XII).

It thus appears that flux systems containing lead are not suitable for the complex fluorides of caesium and chromium. This is unexpected, since

TABLE XI EPMA data for crystals of $Rb_2Cr_5F_{17}$

$Rb_2Cr_5F_{17}$	requires (%)	EPMA indicates (%)
Rb	22.6	23.6
Cr	34.4	34.4
F	42.8	44.1
Pb		0.9
Cl		0.3

as shown in Sections 5.4.1 to 5.4.4, there is little substitution of lead in the caesium iron flourides.

5.11. $BaMF_4$

Attempts to produce crystals of $BaNiF_4$ and $BaCoF_4$ were made, using as fluxes $PbCl_2$, PbF_2, LiBr and CaF_2–$CaCl_2$. Only $PbCl_2$ produced crystals with compositions approximating to $BaMF_4$, as shown in Table XIII. EPMA data indicated that the incorporation of Cl^- and Pb^{2+} were both unusually high, approximately 6% and 3%, respectively. The high chloride content was unexpected, since Cl^- has a much larger ionic radius than F^- (1.8 Å and 1.3 Å, respectively), and the chloride content of fluorides previously grown from $PbCl_2$ or KCl as flux has been very low, as shown in Table XIV. The rather high Pb content was, however, not unexpected since the ionic radius of Ba^{2+} (1.4 Å) is not very different from that of Pb^{2+} (1.3 Å).

5.11.1 (Ba, Pb) Ni (F, Cl)$_4$

A layer of yellow–green, transparent rods up to 6 mm x 2 mm x 0.5 mm grew at the melt surface. The crystals showed simultaneous extinction. The X-ray powder pattern data for (Ba, Pb) Ni (F, Cl)$_4$ showed fair agreement with ASTM data for $BaCoF_4$ [42] but not with ASTM data for $BaNiF_4$ [43].

5.11.2 (Ba, Pb) Co (F, Cl)$_4$

Scarlet rods, up to 3 mm x 0.5 mm x 0.2 mm, were obtained and these showed simultaneous extinction. The X-ray powder pattern of (Ba, Pb) Co (F, Cl)$_4$ was in fair agreement with ASTM data for $BaCoF_4$ [42].

Acknowledgements

The authors are grateful to Dr S. H. Smith and Mr B. J. Garrard for helpful discussions and technical assistance, and to the Mössbauer Group of Liverpool University for information on the Mössbauer spectra of the crystals containing iron. The work was supported in part by the SRC. A. M. and K. Y. wish to thank the British Council and the Japanese Government, respectively, for financial support.

References

1. G. GARTON and B. M. WANKLYN, *J. Crystal Growth* **1** (1967) 49.
2. B. M. WANKLYN, *ibid* **5** (1969) 279.
3. B. M. WANKLYN and B. J. GARRARD, *ibid* **33** (1976) 165.
4. B. M. WANKLYN, *J. Mater. Sci.* **10** (1975) 1487.
5. R. V. COLVIN and S. ARAJS, *J. Phys. Chem. Solids* **26** (1965) 435.
6. A. OKAZAKI, *J. Phys. Soc. Japan* **14** (1959) 1823.
7. P. R. LOCHER, *Solid State Commun.* **5** (1967) 185.
8. J. D. RUSH, A. SIMOPOULOS, M. F. THOMAS and B. M. WANKLYN, *Solid State Commun.* **18** (1976) 1039.
9. G. HEGER and H. DACHS, *Solid State Commun.* **10** (1972) 1299.
10. D. BABEL, F. WALL and G. HEGER, *Z. Naturforsch.* **29b** (1974) 139.
11. A. MAQSOOD and G. P. GUPTA, unpublished work.
12. A. TRESSAUD, F. MENIL, R. GEORGES, J. PORTIER and P. HAGENMULLER, *Mat. Res. Bull.* **7** (1972) 1339.

TABLE XII EPMA data for crystals of (Cs, Pb) CrF_4 and (Cs, Pb)$_2Cr_{4.6}F_{17}$

$(Cs_{0.6}Pb_{0.2})\,CrF_4$	requires (%)	EPMA indicates (%)	$(Cs_{1.55}Pb_{0.45})_2Cr_{4.6}F_{17}$	requires (%)	EPMA indicates (%)
Cs	30.3	31.7	Cs	23.9	23.5
Pb	17.0	17.1	Pb	10.8	10.9
Cr	21.4	21.0	Cr	27.8	29.0
F	31.3	31.2	F	37.5	37.1
Cl		0.1	Cl		0.4

TABLE XIII EPMA data for crystals of (Ba, Pb) Ni(F, Cl)$_4$ and (Ba, Pb) Co (F, Cl)$_4$

	$(Ba_{0.95}Pb_{0.05})Ni(F_{0.89}Cl_{0.11})_4$ requires (%)	EPMA indicates (%)		$(Ba_{0.95}Pb_{0.05})Co(F_{0.89}Cl_{0.11})_4$ requires (%)	EPMA indicates (%)
Ba	46.1	44.7	Ba	46.1	46.9
Pb	3.7	3.8	Pb	3.7	3.0
Ni	20.7	20.9	Co	20.8	20.8
F	24.0	26.3	F	23.9	28.8
Cl	5.5	6.1	Cl	5.5	5.9

TABLE XIV Substitutional flux impurities in fluoride crystals

Crystal formula	Flux	Substitutional Impurity (%)		Reference
	KCl	Cl	K	
CoF_2		< 0.03	< 0.05	[38]
$KCoF_3$		< 0.03		[38]
FeF_2		< 0.03	< 0.05	[38]
$KFeF_3$		< 0.03		[38]
KV_2F_6		0.02		[38]
	$PbCl_2$		Pb	
FeF_3		0.07	< 0.02	[39]
(Co, Fe) F_2		0.03	< 0.02	[39]
$KFeF_3$			0.12	[39]
α $KCrF_4$			0.6	[4]
$K_2Cr_5F_{17}$			0.1	[4]
KVF_4			0.03	[39]
$K_5V_3F_{14}$			< 0.01	[40]
$ZrFeF_6$		< 100 ppm	600 ppm	[41]
Na_2CoFeF_7		0.1	0.3	present work
$Rb_2Cr_5F_{17}$		0.3	0.9	present work
(Cs, Pb) CrF_4		0.1	17.1	present work
(Cs, Pb) $Cr_{4.6}F_{17}$		0.4	10.9	present work
(Ba, Pb) $Ni(F, Cl)_4$		6.1	3.8	present work
(Ba, Pb) $Co(F, Cl)_4$		5.9	3.0	present work

13. R. COSIER, A. WISE, A. TRESSAUD, J. GRANNEC, R. OLAZMAGA and J. PORTIER, *Compt. Rend.* **271** (1970) 142.
14. G. HEGER, *Int. J. Magn.* **5** (1973) 119.
15. D. E. COX, M. EIBSCHÜTZ, H. J. GUGGENHEIM and L. HOLMES, *J. Appl. Phys.* **41** (1970) 943.
16. K. P. BELOV, *et. al., Fiz. Tverd. Tela.* **14** (1970) 2155.
    M. EIBSCHÜTZ, L. HOLMES, H. J. GUGGENHEIM, D. E. COX, *Phys. Rev.* **B6** (1972) 2677.
17. I. N. BELYAEV, O. YA. REVINA, *Russ. J. Inorg. Chem.* (1966) 774.
18. D. ELWELL and H. J. SCHEEL, "Crystal Growth from High Temperature Solutions" (Academic Press, London, 1975).
19. M. SAFA, B. K. TANNER, H. KLAPPER and B. M. WANKLYN, *Phil. Mag.* **35** (1977) 811.
20. M. SAFA, B. K. TANNER, B. J. GARRARD and B. M. WANKLYN, *J. Crystal Growth* **39** (1977) 243.
21. A. TRESSAUD, J. M. DANCE, J. M. PARENTEAU, J. C. LAUNAY, J. PORTIER and P. HAGENMULLER, *ibid* **32** (1976) 211.
22. B. M. WANKLYN, in "Crystal Growth", edited by B. Pamplin (Pergamon, London, 1975).
23. A. TRESSAUD, Thesis Faculte des Sciences de l'Université de Bordeaux, October (1969).
24. G. GARTON, S. H. SMITH and B. M. WANKLYN, *J. Crystal Growth* **13/14** (1972) 588.
25. M. HIDAKA, I. G. WOOD, B. M. WANKLYN and B. J. GARRARD, *J. Phys. Chem.* (in press).
26. A. TRESSAUD, J. PORTIER, R. DE PAPE and P. HAGENMULLER, *J. Solid State Chem.* **2** (1970) 269.
27. A.S.T.M. 27–532.
28. I. MITTEILUNG, F. WALL, G. PAUSEWANG and V. D. BABEL, *J. Less Common Metals* **25** (1971) 257.
29. V. D. BABEL.
30. A.S.T.M. 13–254.
31. A.S.T.M. 24–1079.
32. A.S.T.M; 24–1115.
33. A.S.T.M. 33–673.
34. A.S.T.M. 27–513.
35. A.S.T.M. 26–927.
36. A.S.T.M. 26–364.
37. A.S.T.M. 26–365.
38. B. J. GARRARD, B. M. WANKLYN and S. H. SMITH, *J. Crystal Growth* **22** (1974) 169.
39. W. DAVISON and B. M. WANKLYN, unpublished.
40. B. M. WANKLYN, B. J. GARRARD and F. R. WONDRE, *J. Crystal Growth* **33** (1976) 165.
41. B. J. GARRARD and B. M. WANKLYN, *J. Crystal Growth* (in press).
42. A.S.T.M. 21–65.
43. A.S.T.M. 21–79.

Received 15 August and accepted 2 October 1978.